

# PROPELLER EPI: An MRI Technique Suitable for Diffusion Tensor Imaging at High Field Strength With Reduced Geometric Distortions

Fu-Nien Wang,<sup>1,2</sup> Teng-Yi Huang,<sup>3\*</sup> Fa-Hsuan Lin,<sup>4</sup> Tzu-Chao Chuang,<sup>1</sup> Nan-Kuei Chen,<sup>5</sup> Hsiao-Wen Chung,<sup>1,2</sup> Cheng-Yu Chen,<sup>2</sup> and Kenneth K. Kwong<sup>4</sup>

**A technique suitable for diffusion tensor imaging (DTI) at high field strengths is presented in this work. The method is based on a periodically rotated overlapping parallel lines with enhanced reconstruction (PROPELLER) *k*-space trajectory using EPI as the signal readout module, and hence is dubbed PROPELLER EPI. The implementation of PROPELLER EPI included a series of correction schemes to reduce possible errors associated with the intrinsically higher sensitivity of EPI to off-resonance effects. Experimental results on a 3.0 Tesla MR system showed that the PROPELLER EPI images exhibit substantially reduced geometric distortions compared with single-shot EPI, at a much lower RF specific absorption rate (SAR) than the original version of the PROPELLER fast spin-echo (FSE) technique. For DTI, the self-navigated phase-correction capability of the PROPELLER EPI sequence was shown to be effective for in vivo imaging. A higher signal-to-noise ratio (SNR) compared to single-shot EPI at an identical total scan time was achieved, which is advantageous for routine DTI applications in clinical practice. Magn Reson Med 54:1232–1240, 2005. © 2005 Wiley-Liss, Inc.**

**Key words:** PROPELLER imaging; EPI; geometric distortions; specific absorption rate; diffusion tensor imaging

The importance of diffusion tensor imaging (DTI) in white matter diseases is now well recognized by the clinical neurology community. It has several applications, including the detection of pathologically induced alterations in neural fiber architecture resulting from multiple sclerosis (1), traumatic axonal injury (2), adrenoleukodystrophy (3), or tumors (4,5). The current im-

plementation of DTI often uses single-shot echo-planar imaging (EPI) as the signal readout module following diffusion-weighted (DW) magnetization preparation. Due to strong susceptibility effects from the air–tissue interface, however, the EPI images show severe geometric distortions that are prominent especially near the skull base (6,7). As a consequence, image mapping methods based on DTI, such as fractional anisotropy maps or neural fiber tractograms, are inherently prone to errors in regions such as the frontal lobe near the frontal sinus and optic chiasm in the central brain base.

Reductions in geometric distortions can be accomplished via a decrease in the total data acquisition time following the RF excitation pulse, so as to reduce influences from off-resonance spins. A typical method to achieve this purpose is the multishot EPI or segmented EPI technique, which splits the series of gradient-echo acquisitions into several TRs, at the expense of possible motion artifacts (8). In DW imaging (DWI) using multishot EPI, navigator phase correction is further needed because of phase inconsistencies in the presence of involuntary motion sensitized by the DW gradients (6,7,9). Alternatively, imaging methods based on spin-echo acquisitions are intrinsically immune to off-resonance effects due to the refocusing functions of the 180° pulses. One way to achieve distortion-free DTI images is to use a periodically rotated overlapping parallel lines with enhanced reconstruction (PROPELLER) fast spin-echo (FSE) technique (10–12), which uses multishot FSE acquisitions incorporated with a *k*-space trajectory somewhat similar to that used in the projection reconstruction method (13). Since a relatively large number of 180° pulses are used in PROPELLER FSE, the RF specific absorption rate (SAR) is potentially an issue of concern at high field strengths.

In this article, we propose a PROPELLER EPI technique that is suitable for DTI at high field strengths and reduces geometric distortions. Utilizing our correction procedures, the PROPELLER EPI images simultaneously exhibit substantially reduced geometric distortions compared with single-shot EPI, and much lower SAR than FSE. The method also has a self-phase-correction capability, which is needed in multishot diffusion imaging (14). We will further show that the PROPELLER EPI technique has unique signal-to-noise ratio (SNR) advantages due to a reduced data acquisition window that allows more sampling in *k*-space center to be performed at a fixed total scan time, and hence is beneficial for routine DTI applications.

<sup>1</sup>Department of Electrical Engineering, National Taiwan University, Taipei, Taiwan, R.O.C.

<sup>2</sup>Department of Radiology, Tri-Service General Hospital, Taipei, Taiwan, R.O.C.

<sup>3</sup>Department of Electrical Engineering, National Taiwan University of Science and Technology, Taipei, Taiwan, R.O.C.

<sup>4</sup>MGH/MIT/HMS Athinoula A. Martinos Center for Biomedical Imaging, Massachusetts General Hospital, Charlestown, Massachusetts, USA.

<sup>5</sup>Department of Radiology, Brigham and Women's Hospital, Harvard Medical School, Boston, Massachusetts, USA.

Grant sponsor: National Science Council; Grant numbers: NSC-93-2314-B-002-143; NSC-93-2218-E-011-093; NSC-94-2213-E-011-067. Grant sponsor: National Center for Research Resource; Grant number: P41RR14075; Grant sponsor: National Institutes of Health; Grant numbers: R01-HD040712, R01-NS037462, R03-REB003902A; Grant sponsors: Mental Illness and Neuroscience Discovery (MIND) Institute; Ministry of Education.

Presented in part at the 12th Annual Meeting of ISMRM, Kyoto, Japan, 2004.

\*Correspondence to: Teng-Yi Huang, Ph.D., Assistant Professor, Department of Electrical Engineering, National Taiwan University of Science and Technology, Taipei, Taiwan, R.O.C. E-mail: tyhuang@mail.ntust.edu.tw

Received 27 December 2004; revised 14 June 2005; accepted 28 June 2005. DOI 10.1002/mrm.20677

Published online 3 October 2005 in Wiley InterScience (www.interscience.wiley.com).

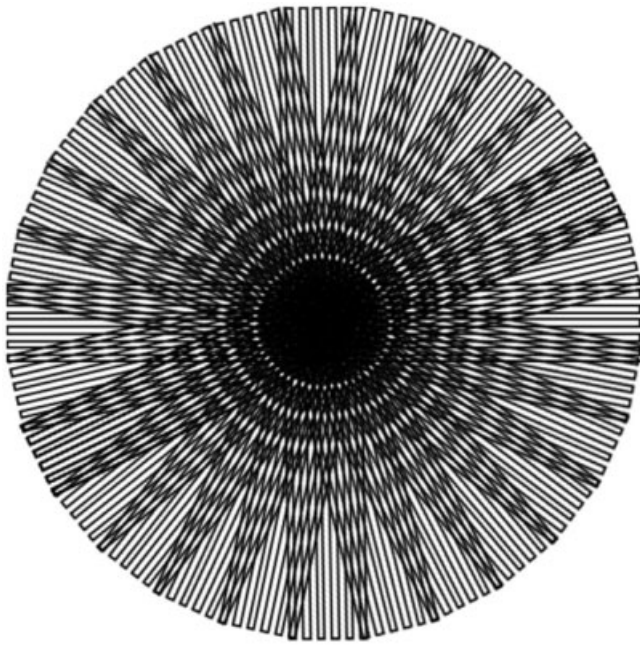


FIG. 1. Schematic  $k$ -space trajectory for PROPELLER imaging. In this study, the data in each blade were acquired using single-shot SE-EPI with 32–44 phase encodings. The blade was then rotated for a certain angle ( $13\text{--}30^\circ$ ) until the data filled the entire circular  $k$ -space. The darker regions reflect data oversampling by different blades.

## MATERIALS AND METHODS

### PROPELLER EPI Sequence

The PROPELLER technique collects data in a series of circularly rotating blades to fill out the entire  $k$ -space (14). The  $k$ -space trajectory is schematically illustrated in Fig. 1. Each blade represents data acquisition from the central  $k$ -space at a certain angle and contains several phase-encoding lines. As opposed to the original PROPELLER technique, which used FSE for signal readout (10,14), we acquired data in each blade using single-shot spin-echo EPI in this study in order to reduce SAR. The timing of the spin echo corresponded to the  $k$ -space center. Isotropic density was used for the distribution of  $k$ -space data throughout this study.

The use of EPI as the signal readout module for PROPELLER imaging naturally results in intrinsically higher sensitivity to off-resonance effects compared to the original version of PROPELLER FSE sequence. We therefore performed a series of correction schemes to reduce possible errors associated with these effects, as detailed below.

### Spatial Registration

An offset of the central reference frequency in EPI acquisition would lead to a global spatial displacement of the reconstructed image along the phase-encoding direction. Since the phase-encoding direction in PROPELLER EPI is changed by a rotation angle in each blade, combining the data without correcting for the spatial displacement may lead to image blurring (10). To reduce possible blurring due to spatial displacements, each blade of the  $k$ -space

data was first Fourier-transformed to a  $128 \times 32$  low-resolution image. All of these low-resolution images were then averaged to one temporary target image. Subsequently, each of the low-resolution images was registered to the temporary target image by calculating the 2D correlation as a function of spatial shifting along different directions. The amount of global spatial displacement for each low-resolution image could thus be determined when a maximum 2D correlation was found. Correction for the displacement was then accomplished by applying the appropriate linear phase shift in  $k$ -space to each blade.

### Phase Correction

Following spatial registration, phase correction was applied to individual blades of  $k$ -space data to ensure constructive data combinations. For this purpose, a pyramid window was first applied to each blade of data in the  $k$ -space, as was done in the original version of PROPELLER FSE imaging (10,14). The resulting phase of the windowed data was then removed from the original unwindowed data in the image domain. The phase-corrected unwindowed data were then used for other corrections, as will be detailed in later sections. Note that this step is required especially for multishot DWI because of the phase changes in every blade due to intravoxel coherent motion in the presence of strong DWI gradients. Otherwise, a destructive combination may result, leading to image artifacts arising from data cancellation.

### Further Reduction of Off-Resonance Effects via Triangular Windowing

A further step to reduce off-resonance effects was done via a weighted adjustment of the  $k$ -space data using a triangular window. The rationale of triangular windowing can be understood by first recalling that for SE-EPI, the central line of the  $k$ -space (i.e., zero phase encoding) corresponds to the time of the SE and hence exhibits the least off-resonance effects. For  $k$ -space lines at a distance from the central  $k$ -space line, the phase accumulation due to off-resonance scales linearly with the time separation from the SE. In other words, the data lines that are far away from the center of  $k$ -space are inherently prone to off-resonance errors, which could lead to spatial displacement along the phase-encoding direction, and hence blurring in PROPELLER imaging. To reduce this blurring effect, we applied a triangular window function to each blade of the  $k$ -space data, which placed more weighting on the central  $k$ -space line, with decreased weighting in a linear fashion according to the distance from the central line along the phase-encoding direction (Fig. 2). Note that since a deemphasis of certain  $k$ -space data would result in possible artifacts due to information loss (15), the triangular windowing operation was performed only for the  $k$ -space data that were oversampled by different blades of the PROPELLER trajectory. In this manner, the combined  $k$ -space data depended more on the signals that were less affected by off-resonance effects, and vice versa.

### Off-Resonance Correction With Field Map

We found that the PROPELLER EPI images had substantially less artifacts due to off-resonance than the conven-

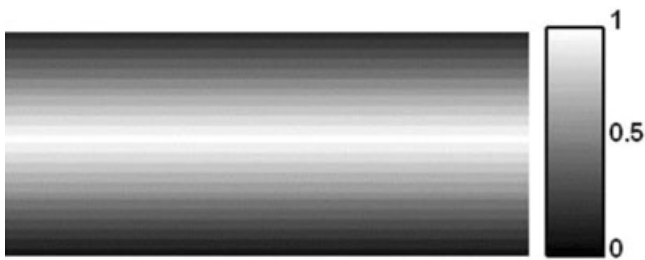


FIG. 2. The triangular window used to reduce off-resonance effects in PROPELLER EPI imaging (frequency encoding along the horizontal direction). Weighting values were varied linearly from 1.0 to 0 toward the outer  $k$ -space along the phase-encoding direction. Emphasis was placed on the central  $k$ -space data because of less off-resonance effects due to SE formation. The windowing operation was performed only for the  $k$ -space data that were oversampled by different blades of the PROPELLER trajectory.

tional single-shot EPI images, for two major reasons: 1) the echo train length in each EPI blade was about four times smaller than that in single-shot EPI imaging, and thus a significant portion of the  $k$ -space data (particularly data at the outer  $k$ -space) contained information that was geometrically less distorted; and 2) spatial registration and triangular windowing were applied (the former reduced global spatial displacement, whereas the latter deemphasized  $k$ -space data that were farther from the time of SE). In our experience, the aforementioned procedures were sufficient to yield satisfactory PROPELLER EPI images under normal shimming conditions. In situations with severe local off-resonance that could lead to prominent image distortions, however, it would be useful to acquire a field map so that the individual image from each EPI blade could be undistorted before the data were combined. For this purpose, we used a scheme proposed by Chen and Wyrwicz (16), which employs several EPI data acquisitions with different TEs to generate a field map for each slice location. Each blade image in PROPELLER EPI was subsequently undistorted according to the field map to reduce the warping effect (16). Note that the acquisition of field maps inevitably increased the total scanning time. Therefore, although we implemented the correction routine, the results shown in this study were mostly obtained without field-map correction, unless otherwise noted.

#### Density Compensation and Data Combination

The combination of data acquired in the different blades was accomplished in  $k$ -space. Following regridding of the  $k$ -space data for each blade (10), density compensation was performed to achieve uniform weighting throughout the entire  $k$ -space. For this purpose, recall first that many of the  $k$ -space data points were acquired more than once due to overlapping blades, with higher data acquisition density near the center of  $k$ -space and lower at the outer  $k$ -space. The numbers of repetitive acquisition were thus recorded for all of the  $k$ -space points. With the effects of triangular windowing taken into account, the numbers of repetitive acquisition became a noninteger representing the accumulated weightings, which were used to divide the  $k$ -space data on a point-by-point basis. After this ma-

nipulation, all data with different  $k$ -space coordinates were equally weighed in terms of signal amplitude. Finally, a PROPELLER EPI image was generated by a Fourier transformation of the appropriately combined  $k$ -space data.

#### Imaging Experiments

A resolution phantom was scanned first demonstrate the feasibility of the PROPELLER EPI technique and its advantages in improving resolution and reducing ghosts. For the phantom, PROPELLER imaging using single-shot SE-EPI was used to acquire 30 blades of  $k$ -space data, each with 44 lines of phase encoding and spaced at  $30^\circ$  from adjacent blades (equivalent to five signal averages, six blades each). The imaging parameters consisted of a TR/TE of 1000/69 ms, 220-mm FOV, 5-mm slice thickness, and a matrix size of  $128 \times 128$ . The total scan time was 30 s. In this part of the study, DWI gradients were not applied.

In addition to the phantom experiments, eight normal subjects were scanned using six-direction DTI with PROPELLER EPI to demonstrate its superiority near the air-tissue interface. The imaging parameters were TR/TE = 1600/70 ms, matrix =  $128 \times 128$ , FOV = 220 mm,  $b$ -factor =  $700 \text{ s/mm}^2$ , slice thickness = 2 mm, and readout bandwidth = 1776 Hz per pixel (maximum), with 16 slices acquired. The echo train length for the single-shot SE-EPI was set to 32 with 128 frequency-encoding points. Note that the TR/TE values were set to the shortest limits under the chosen phase-encoding number to include 16-slice interleaving. Twenty-six blades were acquired for one image for a  $360^\circ$  circular coverage of the  $k$ -space, which corresponded to a rotational angle of  $13.8^\circ$  between adjacent blades. The total scanning time was about 4 min 54 s. Afterwards, conventional six-direction DTI images were acquired using  $128 \times 128$  single-shot EPI, for comparison purposes. The TR/TE values were also set to the shortest limits of 2700/113 ms to include 16-slice interleaving. Fifteen signal averages were used to yield a similar total scan time of 4 min 40 s. Other parameters, such as the voxel dimension, readout bandwidth, and  $b$ -factor, were set identically to those used in PROPELLER EPI imaging. Note that the rationale for choosing these parameters was to compare the SNR and image quality that could be achieved at a routinely acceptable time in clinical practice. In addition, FSE images (TR/TE = 1600/68) at the same slice locations were acquired for comparison of geometry and contrast.

All of the imaging experiments were performed on a head-only 3.0 Tesla MR scanner (Siemens Magnetom Allegra, Erlangen, Germany) with a circularly polarized head coil. The gradient coils have a maximum strength of 40 mT/m. Image reconstruction, including all the correction steps, was performed using MATLAB (Mathworks, Natick, MA, USA) with codes developed in-house on a personal computer with a Pentium III processor.

#### SNR Comparison

An empirical comparison of the SNRs obtained by PROPELLER EPI and single-shot EPI was performed to demonstrate the SNR advantage of PROPELLER EPI due to the

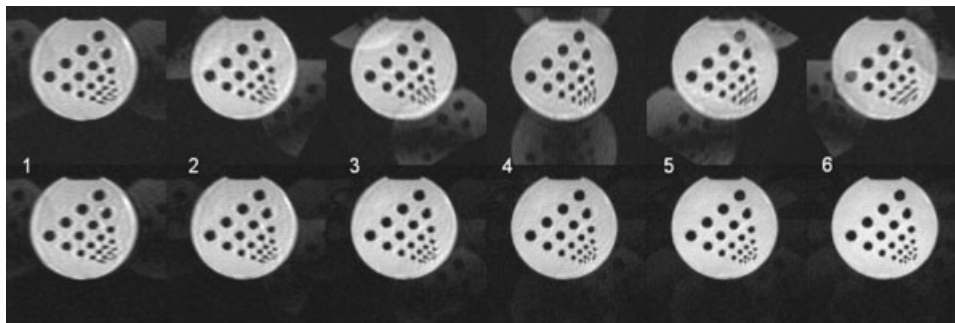


FIG. 3. Step-by-step process of the PROPELLER EPI data combination of the resolution phantom. Top row: Six low-resolution images obtained from direct Fourier transformation of the single-blade  $k$ -space data. Bottom row: Images reconstructed from the combination of one to six (from left to right) blades of data. One first notices from the top row images the anisotropic spatial resolution (as evidenced by the small dots) and the EPI Nyquist ghosts, both of which are oriented differently along the phase-encoding direction. On the bottom row images, both spatial resolution and SNR continually improve as the number of combined blades increases. In addition, the Nyquist ghosts become spread out along different directions and hence become less and less prominent compared to the signal intensity within the phantom. In the final PROPELLER EPI image with six blades, the Nyquist ghosts are barely visible.

reduced data acquisition window, which allows more sampling in  $k$ -space center to be performed at a constant total scan time. For this purpose, regions of interest (ROIs) were selected within the white matter regions and the background from six image slices with  $b = 0$ . The SNR was then taken as the mean of the white matter signal divided by the standard deviation (SD) of the background region. Due to the spatial averaging nature of ROI analysis, the SNR comparison method employed here is restricted to SNR at low spatial resolution. In the particular case of PROPELLER EPI, however, there are serious limitations to such a comparison, which will be addressed in the Discussion section.

## RESULTS

Figure 3 shows the step-by-step process of PROPELLER EPI data combination using the phantom image as an example. The images at the top row are the direct Fourier transformations of single-blade  $k$ -space data from the first to the sixth blade, whereas the bottom row shows images

obtained from the combination of one to six (left to right, respectively) blades of data. In addition to the continual improvements in spatial resolution and SNR in the bottom row images, one can easily notice the Nyquist ghosts, which are obvious in the single-blade images but become effectively reduced in intensity as the number of blades increases. In the final PROPELLER EPI image with the combined six blades of  $k$ -space data, the Nyquist ghosts become barely visible.

Figure 4 demonstrates the effects of phase correction as needed in multishot DWI. One clearly notices the prominent difference between the images obtained without (Fig. 4b) and with (Fig. 4d) phase correction. Note that for multishot DWI using linear phase encoding (such as conventional SE), phase changes due to intravoxel coherent motion in the presence of strong DWI gradients would lead to motion ghosts along the phase-encoding direction. In PROPELLER imaging, on the other hand, artifacts originating from phase changes among different blades are not highly predictable. The image shown in Fig. 4b exhibits only signal cancellation due to destructive data combina-

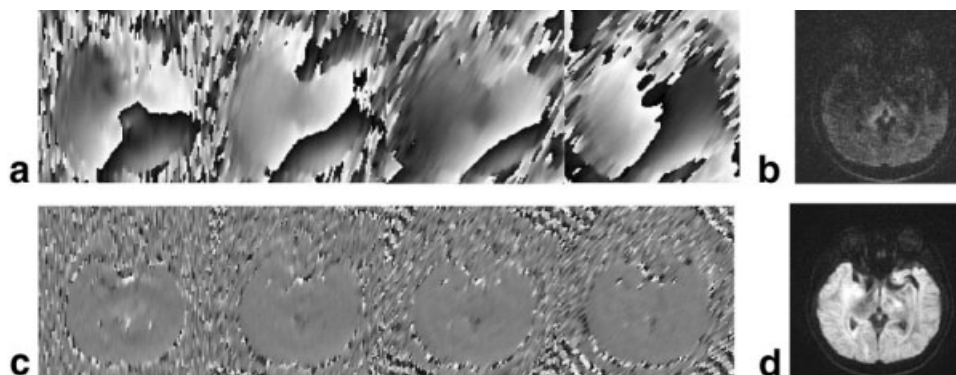


FIG. 4. Comparison of DWI PROPELLER EPI images obtained without and with phase correction. **a:** Phase images from four different blades of data before phase correction. Different phase changes in the individual single-blade phase images due to random intravoxel coherent motion can be seen clearly. **b:** The PROPELLER EPI image without phase correction resulted in nonuniform signal cancellation. **c:** Corrected phase images corresponding to those shown in **a**. **d:** After phase correction, the PROPELLER EPI image shows strong signal intensity with the correct diffusion weighting.

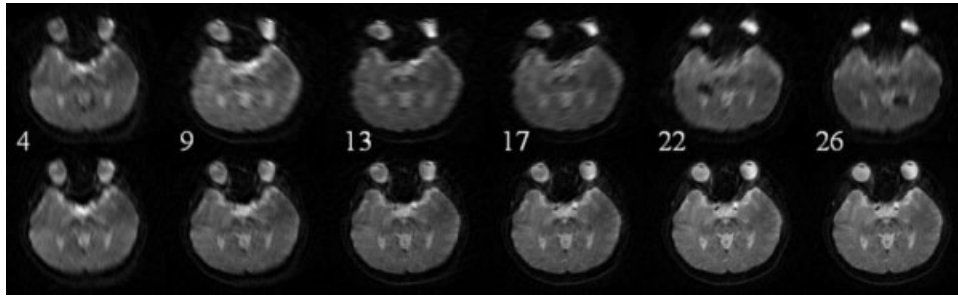


FIG. 5. Step-by-step process of combining PROPELLER EPI data from the human brain at the level of paranasal sinus. Top row: Six low-resolution images obtained from direct Fourier transformation of the single-blade  $k$ -space data. Bottom row: Images reconstructed from the combination of four, nine, 13, 17, 22, and 26 (from left to right) blades of data. The improvements in resolution and SNR are in accordance with the trend shown in Fig. 3 for the phantom. In addition, note that the globe shape of the eyeballs becomes better preserved as the number of data blades increases.

tion. In our experience, we also found other types of artifacts, such as dark bands at various locations, if phase correction was not used.

In a similar fashion to Fig. 3, Fig. 5 shows the step-by-step process of combining PROPELLER EPI data from a human brain image acquired near the paranasal sinus. The images at the top row are the direct Fourier transformations of single-blade  $k$ -space data from the fourth, 9th, 13th, 17th, 22nd, and 26th blades, whereas the corresponding bottom row shows images obtained from the combination of four, nine, 13, 17, 22, and 26 (left to right, respectively) blades of data. The effects in spatial resolution and SNR are consistent with those shown in Fig. 3 for the resolution phantom. In addition, from these brain images it is evident that the globe shape of the eyeballs improves as more blades of data are accumulated. A further comparison is shown in Fig. 6, in which the prominent geometric distortions in the single-shot EPI image (Fig. 6a) are relatively insignificant in the PROPELLER EPI image (Fig. 6b). The FSE image acquired at the same level (Fig. 6c), which is known to be free from off-resonance-related geometric distortions, showed a similar geometric appearance to the PROPELLER EPI image (Fig. 6b). This proves that PROPELLER EPI has good immunity to local off-resonance effects. The PROPELLER EPI image exhibits contrast similar to that of the FSE image at similar TR/TE, whereas the single-shot EPI (Fig. 6a) shows stronger  $T_2$  contrast due to longer TR/TE values.

The effect of triangular windowing is demonstrated in the fractional anisotropy (FA) maps derived from six-direction DTI acquired with PROPELLER EPI (Fig. 7). The frontal lobe of the brain shows image quality improvements with triangular windowing. It is noted, however, that in regions showing severe off-resonance, the use of a shorter data acquisition window and triangular windowing might be inadequate for obtaining high-quality images. In such cases, corrections using field maps would be useful. Figure 8 shows the comparison using phantom images. Note that for this experiment, a much longer data acquisition window (matrix size =  $256 \times 64$  for a single blade) was intentionally used in PROPELLER EPI to magnify the off-resonance effects. In other words, in the presence of severe off-resonance, triangular windowing alone (Fig. 8c) would be unable to give a satisfactory performance. Field map correction was shown to give good results with substantially reduced blurring (Fig. 8d). The expense was the longer scan time required to obtain a reliable field map (16).

Figure 9 shows two series of color-coded FA maps derived from six-direction DTI images acquired using single-shot EPI and PROPELLER EPI. The advantage of PROPELLER EPI in the relative absence of geometric distortions can be seen clearly in the frontal lobe, as well as in the adjacency of the air-tissue interface. Since the susceptibility-induced distortions worsen as the static magnetic field increases, the avoidance of geometric distortions using

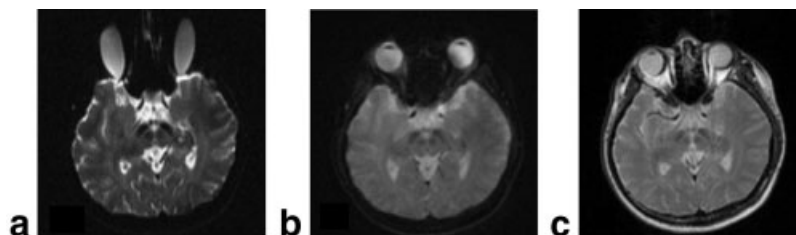
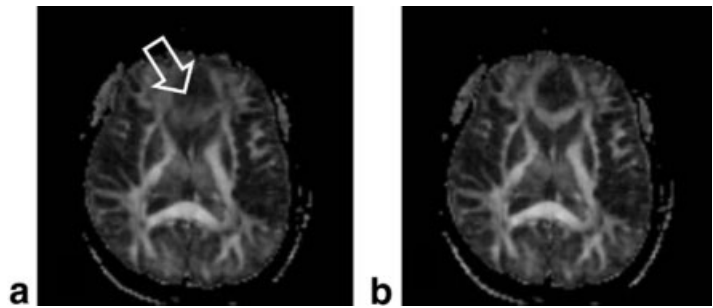


FIG. 6. Axial images of the human brain in vivo acquired using single-shot EPI (a), PROPELLER EPI (b), and FSE (c) techniques, all obtained with  $T_2$  contrast but without diffusion weighting ( $b = 0$ ). Note the warped eyeballs in Fig. 6a caused by susceptibility-induced off-resonance near the paranasal sinus. The geometric distortion of the eyeballs was substantially reduced in PROPELLER EPI via a shortening of the total data readout time within one single RF excitation. The resulting image shown in b exhibits a nearly identical shape compared to the FSE image in c.

FIG. 7. FA maps derived from six-direction DTI acquired using PROPELLER EPI without (a) and with (b) triangular windowing to further reduce the influences from off-resonance effects. The genu of the corpus callosum in a (open arrow) was somewhat obscured with seemingly lowered anisotropy, which may suggest infiltrative pathology. On the other hand, b shows better quality and normal genu of the corpus callosum with the use of triangular windowing.



methods such as the PROPELLER EPI proposed in our study becomes increasingly important at high fields.

An empirical comparison of DWI images obtained at  $b = 700 \text{ s/mm}^2$  showed that the SNR of PROPELLER EPI was slightly better than single-shot EPI (about 20–30%) at a similar total scan time of about 5 min, using an ROI analysis. Figure 10 shows the image comparison, in which the SNR advantage of the PROPELLER EPI is visually evident. Note, however, that the SNR gain reported here is largely empirical, as the scanning parameters in these two types of EPI sequences were not kept constant. The single-shot EPI had longer a TR and TE (i.e., a stronger  $T_2$  weighting) compared to the situation of PROPELLER EPI, where  $T_1$  relaxation played a greater role in the determination of the signal intensity. In this study, the TR/TE values were chosen such that their minimal allowable values were reached with the least amount of system idle time. If TR/TE were fixed for the two EPI sequences, the comparison would be in favor of single-shot EPI because the amount of data sampled (particularly at the outer  $k$ -space) would be substantially larger compared to PROPELLER EPI. In practice, since the data acquisition window within one RF excitation was significantly shortened in PROPELLER EPI, the resulting system idle time allowed either more slices to be interleaved within one TR, or a shortening of TR/TE to yield higher SNR. Certainly in the latter case (as was done in our study), the consequent changes in image contrast made the SNR comparison somewhat subjective. In other words, the comparison performed in this study was based on practical considerations as would be encountered in clinical applications.

## DISCUSSION

In this article we have presented the implementation of a PROPELLER EPI acquisition sequence and its correspond-

ing image reconstruction methods. In comparison with the original version of PROPELLER imaging proposed by Pipe (14), which used FSE as the signal readout module, PROPELLER EPI has the following advantages: First of all, PROPELLER EPI exhibits much lower SAR than PROPELLER FSE due to the absence of long  $180^\circ$  pulse trains. Particularly at high field strengths, the SAR in the context of patient safety is an essential factor that should be taken into serious consideration. Second, PROPELLER EPI allows much easier multislice interleaving within one TR because there is less cross talk than would be brought about by the imperfect slice profiles of the selective  $180^\circ$  pulses (17). This advantage is especially useful in clinical practice, where multislice imaging is highly desirable. Third, since there are no repetitive  $180^\circ$  refocusing pulses in PROPELLER EPI, echo spacing is consequently much shorter than in PROPELLER FSE. As a result, whole-brain coverage with a larger number of contiguous slices interleaved in one TR becomes easily feasible.

Compared with single-shot EPI, the PROPELLER EPI scheme proposed in our work may seem to be less efficient in terms of  $k$ -space coverage. After all, PROPELLER EPI is multishot in nature, and thus may not be appropriate for fast scanning applications such as dynamic susceptibility-contrast perfusion-weighted imaging. Nevertheless, PROPELLER EPI provides a unique feature of substantially reduced geometric distortions near the air-tissue interfaces that are prone to susceptibility effects. This advantage originates from a combination of the reduced number of phase encodings (and hence shorter readout time) in one single blade, and the radial nature of  $k$ -space traversal. Unlike single-shot EPI, where the filling of  $k$ -space is achieved by a continuous lengthening of the acquisition window, a substantial portion of the  $k$ -space (particularly the outer part) in PROPELLER EPI is filled with different blades of an acquisition in which a shorter acquisition

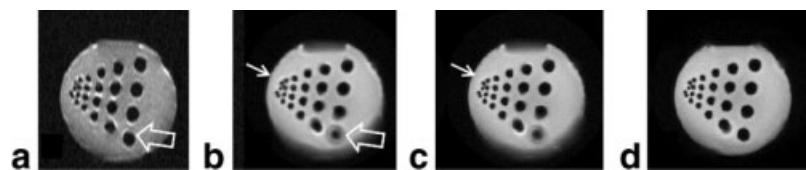


FIG. 8. Effectiveness of field map correction in PROPELLER EPI in the presence of severe off-resonance. a: Image reconstructed from one single blade ( $256 \times 64$ ) of data. The phase-encoding direction was vertical. With the intentional increase of the matrix size to  $256 \times 64$ , the data acquisition window was lengthened and hence the off-resonance effects were magnified. The warping of the phantom along the phase-encoding direction led to blurring in b (open arrows), which was obtained with generic PROPELLER reconstruction. With triangular windowing (c), the blurring was improved slightly (arrows). With triangular windowing plus field map correction (d), the blurring was largely eliminated.

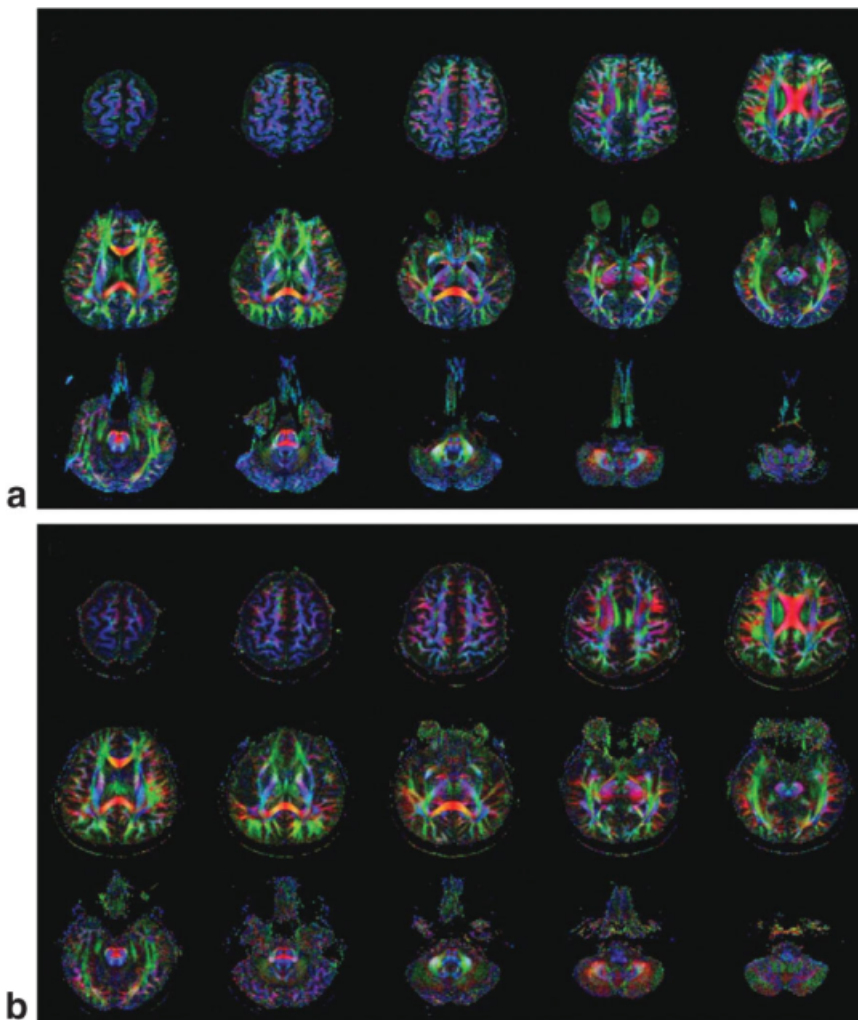


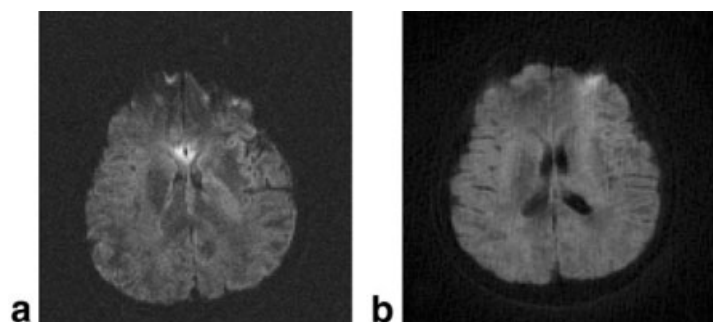
FIG. 9. Color-coded FA maps (red: left-right; green: anterior-posterior; blue: superior-inferior) corresponding to 15 slice locations in a 28-year-old healthy subject, derived from six-direction diffusion-tensor-weighted images acquired using single-shot EPI (a) and PROPELLER EPI (b) at  $b = 700$   $\text{s}/\text{mm}^2$ . Note the major difference in the amount of geometric distortions in the frontal lobe, near the paranasal sinus, and near the skull base. Some of the white matter fiber bundles, such as the corticospinal tracts, are more easily identifiable from PROPELLER EPI color-coded FA maps that are relatively free from distortions.

window is used. During the data combination process, therefore, information close to the time of SE can be integrated to form the image with reduced geometric distortions (cf., Fig. 5). As for the motion-freezing capability, although admittedly it is no better than ultrafast single-shot EPI, the self-navigation property of PROPELLER EPI (10,14) could compensate for the motion influences at least to some extent.

An application for which PROPELLER EPI is particularly suitable is white matter tractography based on DTI (1–3,18,19). In tractography using DTI, whole-brain coverage with contiguous slices is desirable, which makes PRO-

PELLER EPI attractive due to the absence of a large number of  $180^\circ$  pulses. In addition, multiple signal averages are needed in DTI for tractography in order to achieve high SNR for reliable information on neural fiber orientations (20,21). Here the multishot nature of PROPELLER  $k$ -space trajectory provides SNR advantages due to the repeated sampling of the central  $k$ -space. With similar total scan times that are clinically acceptable (say around 5 min), the shortened data acquisition window within individual blades in PROPELLER EPI leads to a shortening of TR and TE, and hence allows more signal sampling in  $k$ -space center compared to single-shot EPI. Equivalently speaking,

FIG. 10. Single-shot EPI image (a: TR/TE = 2700/113, 15 averages) and PROPELLER EPI image (b: TR/TE = 1600/70, 26 blades) acquired with diffusion weighting at  $b = 700$   $\text{s}/\text{mm}^2$  and with similar total scan times that are clinically acceptable (about 5 min). The PROPELLER EPI showed better SNR, at the same time, with less geometric distortions.



considering SNR measured with low-resolution (e.g., measured with ROI), PROPELLER EPI has higher SNR than single-shot EPI, because of the larger percentage of the scan time spent in traversing through the central  $k$ -space. This factor alone helps to improve the image SNR. In our study, DWI PROPELLER EPI showed a higher empirical SNR compared to single-shot EPI with the same diffusion weighting.

Other than the oversampling of the central  $k$ -space, however, the SNR benefit of PROPELLER EPI as compared to single-shot EPI at similar total scan times is quantitatively rather complex. Due to nonuniform signal averages in different portions of the  $k$ -space, the SNR in PROPELLER EPI is obviously “colored,” being larger at the central portion of the  $k$ -space and lower at the outer  $k$ -space, respectively. The ROI SNR analysis performed in this study, which actually measured SNR at a low spatial resolution, thus somehow favored the PROPELLER EPI technique. In other words, oversampling of the central  $k$ -space only benefits SNR at low spatial resolution. In addition, considering that the  $k$ -space coverage is circular instead of rectangular, as is commonly encountered in single-shot EPI, the voxel size difference further complicates an objective comparison. Furthermore, the shortened TR and TE in PROPELLER EPI have opposite effects on SNR due to  $T_1$  and  $T_2$  relaxation. Taking, for example, the white matter that is essential for DTI, with  $T_1$  on the order of 900 ms at 3.0 Tesla (22), a change in TR from 2700 to 1600 would result in a 12% (or factor of 0.88) signal decrease. Yet for  $T_2$  of the white matter on the order of 100 ms, a reduced TE from 113 ms to 70 ms would lead to an SNR increase by a factor of 1.54, which well compensates for the SNR loss caused by the shortened TR. On the other hand, the use of triangular windowing results in some SNR loss in that the effective number of oversampling of the central  $k$ -space becomes reduced, which may somehow diminish the SNR benefits due to changes in TR/TE. To make the comparison even more difficult, note that the derivation of the noise level is quite different in single-shot EPI and PROPELLER EPI images. In single-shot EPI images, one would measure the noise level in an ROI defined within the background region, while avoiding the inclusion of the Nyquist ghost. In PROPELLER EPI images, however, the Nyquist ghosts are spread over the entire circular FOV, such that it is virtually impossible to measure pure random noise without including the Nyquist ghosts. Certainly, a detailed quantification of the actual SNR advantage of PROPELLER EPI depends on the number of blades, the echo train length used in one blade, and a lot more factors than those addressed in this discussion. It was thus beyond the scope of this study, in which only simplified calculations were performed.

It should be noted that although the PROPELLER EPI images are in general free from prominent susceptibility-induced geometric distortions, its use of a shorter data acquisition window does not remove the distortions completely (23). This is understood in that even a slight image warping along the phase-encoding direction in each EPI blade could lead to circular blurring after the PROPELLER data are combined (cf., Fig. 7). Therefore, in cases in which severe off-resonance effects are present, or when high spatial resolution necessitating a large matrix size is desired,

correction schemes employing field map acquisition would be needed (16). Since the acquisition of accurate field maps takes time, involuntary motion between scans may become an issue and reduce the effectiveness of the field map correction. Other approaches, such as parallel imaging methods using phased array receiver coils, could further reduce the number of phase encodings to decrease the extent of susceptibility artifacts (24). An investigation of PROPELLER EPI with parallel imaging is currently underway (25).

We conclude that the PROPELLER EPI is an effective technique that combines the advantages of reduced geometric distortions compared to single-shot EPI, and substantially lower SAR compared to PROPELLER FSE. In addition, its multislice interleaving compatibility, better SNR, and self-navigated phase-correction capability make it very attractive for DTI applications. It is particularly suitable for high-field imaging and thus may be clinically useful at 3.0 Tesla.

## ACKNOWLEDGMENTS

F.N.W. and T.Y.H. received support from the National Science Council and the Ministry of Education, respectively, under the International Student Exchange program.

## REFERENCES

1. Guo AC, MacFall JR, Provenzale JM. Multiple sclerosis: diffusion tensor MR imaging for evaluation of normal-appearing white matter. *Radiology* 2002;222:729–736.
2. Arfanakis K, Haughton VM, Carew JD, Rogers BP, Dempsey RJ, Meyerand ME. Diffusion tensor MR imaging in diffuse axonal injury. *AJNR Am J Neuroradiol* 2002;23:794–802.
3. Ito R, Melhem ER, Mori S, Eichler FS, Raymond GV, Moser HW. Diffusion tensor brain MR imaging in X-linked cerebral adrenoleukodystrophy. *Neurology* 2001;56:544–547.
4. Boujraf S, Luypaert R, Shabana W, De Meirleir L, Sourbron S, Osteaux M. Study of pediatric brain development using magnetic resonance imaging of anisotropic diffusion. *Magn Reson Imaging* 2002;20:327–336.
5. Mori S, Frederiksen K, van Zijl PC, Stieltjes B, Kraut MA, Solaiyappan M, Pomper MG. Brain white matter anatomy of tumor patients evaluated with diffusion tensor imaging. *Ann Neurol* 2002;51:377–380.
6. Li Z, Wu G, Zhao X, Luo F, Li SJ. Multiecho segmented EPI with z-shimmed background gradient compensation (MESBAC) pulse sequence for fMRI. *Magn Reson Med* 2002;48:312–321.
7. Jiang H, Golay X, van Zijl PC, Mori S. Origin and minimization of residual motion-related artifacts in navigator-corrected segmented diffusion-weighted EPI of the human brain. *Magn Reson Med* 2002;47:818–822.
8. Kim SG, Hu X, Adriany G, Ugurbil K. Fast interleaved echo-planar imaging with navigator: high resolution anatomic and functional images at 5 Tesla. *Magn Reson Med* 1996;35:895–902.
9. Brockstedt S, Moore JR, Thomsen C, Holtas S, Stahlberg F. High-resolution diffusion imaging using phase-corrected segmented echo-planar imaging. *Magn Reson Imaging* 2000;18:649–657.
10. Pipe JG, Farthing VG, Forbes KP. Multishot diffusion-weighted FSE using PROPELLER MRI. *Magn Reson Med* 2002;47:42–52.
11. Forbes KP, Pipe JG, Karis JP, Heiserman JE. Improved image quality and detection of acute cerebral infarction with PROPELLER diffusion-weighted MR imaging. *Radiology* 2002;225:551–555.
12. Forbes KP, Pipe JG, Karis JP, Farthing V, Heiserman JE. Brain imaging in the unsedated pediatric patient: comparison of periodically rotated overlapping parallel lines with enhanced reconstruction and single-shot fast spin-echo sequences. *AJNR Am J Neuroradiol* 2003;24:794–798.
13. Lauterbur PC. Image formation by induced local interactions: examples employing nuclear magnetic resonance. *Nature* 1973;242:190.

14. Pipe JG. Motion correction with PROPELLER MRI: application to head motion and free-breathing cardiac imaging. *Magn Reson Med* 1999;42: 963–969.
15. Arfanakis K, Tamhane AA, Pipe JG, Anastasio MA. k-Space undersampling in PROPELLER imaging. *Magn Reson Med* 2005;53:675–683.
16. Chen NK, Wyrwicz AM. Optimized distortion correction technique for echo planar imaging. *Magn Reson Med* 2001;45:525–528.
17. Joseph PM, Axel L, O'Donnell M. Potential problems with selective pulses in NMR imaging systems. *Med Phys* 1984;11:772–777.
18. Basser PJ, Pajevic S, Pierpaoli C, Duda J, Aldroubi A. In vivo fiber tractography using DT-MRI data. *Magn Reson Med* 2000;44:625–632.
19. Mori S, Crain BJ, Chacko VP, van Zijl PC. Three-dimensional tracking of axonal projections in the brain by magnetic resonance imaging. *Ann Neurol* 1999;45:265–269.
20. Jones DK. Determining and visualizing uncertainty in estimates of fiber orientation from diffusion tensor MRI. *Magn Reson Med* 2003;49:7–12.
21. Basser PJ, Pajevic S. Statistical artifacts in diffusion tensor MRI (DT-MRI) caused by background noise. *Magn Reson Med* 2000;44: 41–50.
22. Parry A, Clare S, Jenkinson M, Smith S, Palace J, Matthews PM. White matter and lesion T1 relaxation times increase in parallel and correlate with disability in multiple sclerosis. *J Neurol* 2002;249:1279–1286.
23. McKinnon GC. Ultrafast interleaved gradient-echo-planar imaging on a standard scanner. *Magn Reson Med* 1993;30:609–616.
24. Yang QX, Wang J, Smith MB, Meadowcroft M, Sun X, Eslinger PJ, Golay X. Reduction of magnetic field inhomogeneity artifacts in echo planar imaging with SENSE and GESEPI at high field. *Magn Reson Med* 2004;52:1418–1423.
25. Chuang TC, Huang TY, Lin FH, Wang FN, Chung HW, Chen CY, Kwong KK. PROPELLER EPI with SENSE parallel imaging using a circularly symmetric phase array RF coil. In: Proceedings of the 12th Annual Meeting of ISMRM, Kyoto, Japan, 2004.